Surface-enhanced alloy effects on $Hg_{1-x}Cd_xTe(100)$ surface states and the site-dependent coherent-potential approximation

Garnett W. Bryant
McDonnell Douglas Research Laboratories, P.O. Box 516, Saint Louis, Missouri 63166
(Received 6 November 1986)

The surface states of ideal, (100) cation- and anion-terminated surfaces of $Hg_{1-x}Cd_xTe$ ($x=0$, 0.2, 0.5, 0.8, 1.0) have been determined by use of the site-dependent coherent-potential approximation (SDCPA) for the alloy. Alloy effects are more important for localized states than for well-extended states and are greatly enhanced for states that are sensitive to the cation sites and localized to a cation surface. In the alloy, the localized states sensitive to the disorder have the character of the alloy constituents rather than of some average, effective constituent. The ideal cation surface has HgTe- and CdTe-like surface-state bands between the valence and conduction bands but no virtual-crystal-related surface-state features in this energy range. Both constituentlike bands exist for each alloy composition except $x=0$ or 1.0. Anion surface states and back-bonded surface states occurring below the valence-band edge do not exhibit this bimodal character because these states are less sensitive to the cation sites. The coherent-potential-approximation (CPA) self-energy at a cation-surface site is also very different from those in the bulk or near anion surfaces as a result of the surface-enhanced alloy effects. For comparison with the SDCPA, we also present results obtained with the virtual-crystal approximation and with the bulk CPA (same self-energy at all sites). Only the SDCPA yields a qualitatively correct description of all the states considered.

I. INTRODUCTION

Alloy effects on the electronic structure of a compound semiconductor alloy depend on how similar the constituents are, how sensitive the states are to fluctuations in local environment, and how sensitive the states are to the disordered sites. The bulk states of III-V semiconductor alloys, such as $Ga_{1-x}Al_xAs$, are well described by the virtual-crystal approximation (VCA), in which a composition-weighted average cation potential defines the effective cation potential, because the constituent cations are similar. In the II-VI alloy $Hg_{1-x}Cd_xTe$, the alloy constituents, HgTe and CdTe, are very different. Relativistic effects present in HgTe but weak in CdTe (Refs. 1–3) lower the Hg $6s$ level to such a degree in relation to the Te $5p$ states that HgTe has a zero band gap and an inverted band structure while CdTe has the normal, semiconductor level ordering. Despite the differences between HgTe and CdTe, the alloy bulk density of states (DOS) near the valence-band maximum predicted by the VCA is identical to the DOS predicted by the more sophisticated coherent-potential approximation (CPA). These valence states are anion-derived and only weakly perturbed by alloy disorder. Even the conduction-band states near the conduction-band minimum, which are cation-derived, are well described by the VCA (the CPA predicts a small additional band-gap narrowing[1,2]). These conduction-band states are well extended, sample many sites, and average over fluctuations in the local environment. However, away from the band edges the bulk states are more local in character and differences between the VCA and CPA are important. For example, CPA calculations for the alloy density of states of deep valence states[1,2] display atomiclike HgTe and CdTe features not predicted by the VCA but observed by photoemission.[1]

Intuition suggests and model calculations[4–7] confirm that states localized to surfaces or defects are more sensitive to local alloy configurations than are well-extended bulk states and require, in an alloy like $Hg_{1-x}Cd_xTe$, a sophisticated alloy approximation. Recently we reported[8] on the first generalized site-dependent coherent-potential-approximation (SDCPA) calculation of the surface states of a real semiconductor alloy such as $Hg_{1-x}Cd_xTe$. The local densities of states at ideal (100) cation- and anion-terminated surfaces and in the bulk of $Hg_{1-x}Cd_xTe$ ($x=0.5$) were determined. The CPA self-energy was site-dependent near the surface because the surface breaks the translational symmetry of the lattice. Our results confirmed that alloy effects on states localized, in our case, to cation surfaces and sensitive to the cation sites are greatly enhanced. The alloy cation surface DOS has both HgTe- and CdTe-like bands of states but no virtual-crystal-related features. Similar bimodal structure was seen in the deep valence states.[1,2] Use of the generalized SDCPA was essential to account for the surface-enhanced alloy effects. Previous realistic calculations[9–16] of surface and defect states in semiconductor alloys have used the VCA. None of these calculations could reproduce the bimodal structure seen in our results.

We have extended the work previously reported for $x=0.5$, where alloy effects should be most severe, to consider alloys with larger and smaller x. For all alloy compositions considered, the surface-enhanced alloy effects are significant and the surface states display the bimodal character seen for $x=0.5$. The (100)-cation-surface states of $Hg_{1-x}Cd_xTe$ continue to be either HgTe-like or CdTe-like but not virtual-crystal-like even for low concentrations of the minority constituent. The minority band disappears only when the minority constituent is absent. Localization of the states in just one dimension, i.e., nor-

 ©1987 The American Physical Society

mal to the surface, is enough to ensure that states which are sensitive to the cation disorder will be constituentlike rather than virtual-crystal-like.

In this paper we will present a more detailed discussion of the calculations and additional results from our study at $x=0.5$ which were not discussed previously,[8] and we will extend the work to larger and smaller x. Results for both cation and anion (100) surfaces and for surface states in the fundamental gap and deep in the valence band will be presented. Comparisons will be made among calculations performed with different alloy models to illustrate the reliability of each. The sensitivity of the results to the form chosen for the CPA self-energy will also be discussed. The calculations will be presented in Sec. II, the results in Sec. III, and conclusions in Sec. IV.

II. THEORY

A. The tight-binding models

We use tight-binding (TB) models to describe the alloy constituents. Because these models are fitted to reproduce bulk band properties, extrapolating the models to studies of localized states must be done carefully, especially in alloy systems where fluctuations in local environment can be significant. We chose to use the second-nearest-neighbor TB Hamiltonians developed by Hass *et al.*[2] to describe HgTe and CdTe. Spin-orbit effects are included by using a 16-state model with cation and anion s and p states for each spin. Hass *et al.* chose the energy levels to be the atomic energies and determined the off-diagonal elements by fitting to experimental energy gaps and pseudopotential calculations. In the model of Hass *et al.*, the Te energy levels in HgTe and CdTe are chosen to be the same, as one would expect, provided that charge-transfer effects are small. Other TB models[14,15,17] have also been developed for HgTe and CdTe by fitting predicted band structures to experimental energy gaps. However, the model of Hass *et al.* should describe localized states better than the other TB models in which the anion energy levels change as much between HgTe and CdTe as the cation levels change even though the anion is the same.

The TB models of Hass *et al.*, as well as the other TB models for HgTe and CdTe, predict conduction-band masses that are too large. However, that discrepancy can be corrected. We generalized the model of Hass *et al.* by including couplings previously ignored to obtain more accurate conduction bands and masses. The new off-diagonal couplings we include are $[E_{sx}(110)]_{aa}$ and $[E_{sx}(110)]_{cc}$, the coupling between the s level on one anion (cation) and those p levels on an adjacent anion (cation) that are not perpendicular to the line joining the two anions (cations). The band energies at the band edges do not change when $[E_{sx}(110)]_{aa}$ and $[E_{sx}(110)]_{cc}$ are varied. However, the lowest two conduction bands and the split-off band do change away from the band edges when $[E_{sx}(110)]_{aa}$ and $[E_{sx}(110)]_{cc}$ are varied. Thus, the new off-diagonal elements can be adjusted to provide better conduction-band masses without losing the agreement with experimental band gaps. Avoided crossings between the lower two conduction bands along the X direction are predicted by pseudopotential calculations.[18] These avoided crossings are also predicted by use of the TB model with the new off-diagonal elements but not by use of the model without the new elements. Thus use of the TB model with the extra off-diagonal elements improves the band structure near the conduction-band edge and predicts the sharp structure in the density of states several eV above the band edge due to the avoided crossings. Comparisons of the band structures of HgTe and CdTe calculated with and without the new parameters are shown in Fig. 1. The conduction-band effective masses in the X (L) direction, predicted by using $[E_{sx}(110)]_{aa}=[E_{sx}(110)]_{cc}=0$, are $m_{\mathrm{HgTe}}=0.051m_0$ $(0.063m_0)$ and $m_{\mathrm{CdTe}}=0.209m_0$ $(0.212m_0)$. With $[E_{sx}(110)]_{aa}=[E_{sx}(110)]_{cc}=-0.125$ eV, the masses are $m_{\mathrm{HgTe}}=0.028m_0$ $(0.035m_0)$ and $m_{\mathrm{CdTe}}=0.099m_0$ $(0.101m_0)$. The experimental masses[19,20] are $m_{\mathrm{HgTe}}=0.028m_0$ and $m_{\mathrm{CdTe}}=0.11m_0$. Using band structures which give the correct conduction-band masses near the band edge and the correct structure several eV from the edge is important in our calculations since the surface states most sensitive to alloy disorder are derived from the conduction-band states. The parameters used in the TB models of

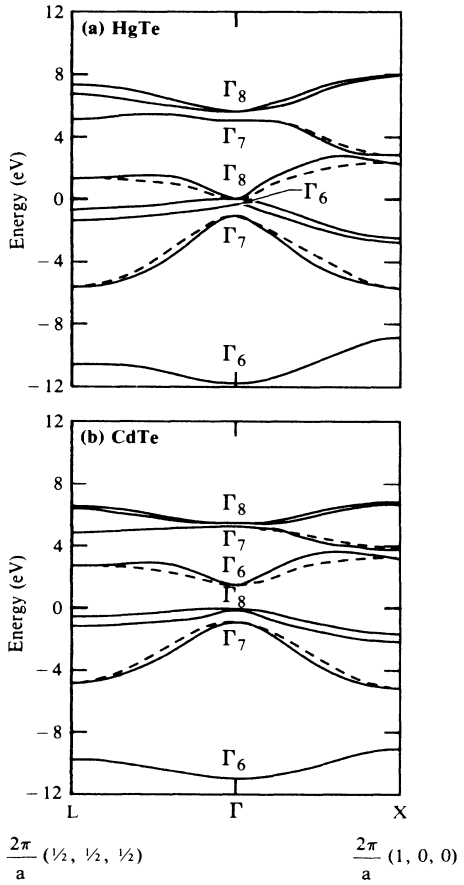

FIG. 1. Bulk band structure for (a) HgTe and (b) CdTe calculated using the model of Hass *et al.* (dashed curves) and the model of Hass *et al.* with the extra couplings (solid curves).

Hass *et al.* are listed in Table I. The notation is that of Ref. 21.

B. The alloy model

The alloy disorder effects are incorporated into the calculations by using effective medium models. In this approach the randomly occupied cation sites are occupied by effective atoms. In the VCA the effective atom is defined by using the compositionally weighted average of the HgTe and CdTe parameters listed in Table I. As mentioned in the Introduction, the VCA should work well when the constituents are similar, and can even work well for dissimilar constituents like HgTe and CdTe if the states are well extended or insensitive to cation sites. Hass *et al.* chose the anion diagonal terms to be identical for the two constituents and the off-diagonal terms of the two to be nearly the same. Thus, the VCA is assumed to be adequate for the anion diagonal elements and the off-diagonal elements. The VCA values are used for these matrix elements in all calculations reported here.

The cation diagonal elements must be modeled more carefully. The VCA can be used for these matrix elements to describe well-extended states but not localized states sensitive to the large difference between Hg and Cd s-energy levels ($E_{\mathrm{Hg}\,s}=-1.32$ eV and $E_{\mathrm{Cd}\,s}=0.12$ eV).

TABLE I. The tight-binding parameters of Hass *et al.* for HgTe and CdTe. The last two parameters are introduced in this work.

Parameter	HgTe (eV)	CdTe (eV)
$[E_{ss}(000)]_{aa}$	−9.00	−9.00
$[E_{ss}(000)]_{cc}$	−1.32	0.12
$[E_{xx}(000)]_{aa}$	0.10	0.10
$[E_{xx}(000)]_{cc}$	4.11	4.34
λ_a	0.375	0.34
λ_c	0.265	0.04
$[E_{ss}(\frac{1}{2}\frac{1}{2}\frac{1}{2})]_{ac}$	−1.036	−1.121
$[E_{sx}(\frac{1}{2}\frac{1}{2}\frac{1}{2})]_{ac}$	0.343	0.330
$[E_{sx}(\frac{1}{2}\frac{1}{2}\frac{1}{2})]_{ca}$	1.070	1.103
$[E_{xx}(\frac{1}{2}\frac{1}{2}\frac{1}{2})]_{ac}$	0.514	0.534
$[E_{xy}(\frac{1}{2}\frac{1}{2}\frac{1}{2})]_{ac}$	1.229	0.955
$[E_{ss}(110)]_{aa}$	−0.086	−0.01
$[E_{ss}(110)]_{cc}$	−0.062	−0.033
$[E_{sx}(011)]_{aa}$	−0.30	−0.10
$[E_{sx}(011)]_{cc}$	−0.18	−0.10
$[E_{xx}(110)]_{aa}$	0.13	0.12
$[E_{xx}(110)]_{cc}$	0.16	0.073
$[E_{xx}(011)]_{aa}$	−0.17	−0.10
$[E_{xx}(011)]_{cc}$	−0.15	−0.10
$[E_{xy}(110)]_{aa}$	0.25	0.15
$[E_{xy}(110)]_{cc}$	0.20	0.15
$[E_{sx}(110)]_{aa}$	−0.125	−0.125
$[E_{sx}(110)]_{cc}$	−0.125	−0.125

To provide a better model for the cation diagonal disorder, we use the coherent-potential approximation. In the CPA, the cation s levels are described by self-energies, $\Sigma_{\uparrow\uparrow}(\omega)$ and $\Sigma_{\downarrow\downarrow}(\omega)$, for each spin and spin-mixing terms $\Sigma_{\uparrow\downarrow}(\omega)$ and $\Sigma_{\downarrow\uparrow}(\omega)$; and, in principle, similar self-energies for the cation p levels and the coupling between cation s and p levels. As mentioned, all anion diagonal terms and the interatomic hopping terms are treated with the VCA. The s self-energy at a specific cation site is energy-dependent and represents the effective s energy-level of the cation site that an electron with energy ω experiences when scattering from that site in the alloy. The real part of the self-energy gives the energy level and the imaginary part gives the broadening. The self-energies are determined by requiring that the effective cation produce the same scattering of an electron with energy ω as the average scattering of Hg and Cd embedded in the effective medium.[22,23]

All bulk, cation sites are equivalent so the same self-energy can be used for each bulk site. However, near a surface, translational symmetry is broken and the self-energy should be site-dependent. As a consequence, near a surface a self-consistent self-energy must be found for each plane of equivalent sites. Moreover, the self-energy for a given plane depends on the self-energies of other planes because these other self-energies determine the carrier propagation through the alloy. Berk[4] was the first to use the site-dependent CPA to study the surface states of a cleaved, alloy surface. Other model calculations[5,6,24,25] and realistic calculations[8] confirm that the site dependency must be included to adequately model the surface states.

The bulk CPA is normally implemented by ignoring the coupling between s and p levels in the self-energy, the off-diagonal terms that mix spins, and the spin dependence of the diagonal terms. However, because the surface normal defines a special direction, there is no reason to neglect spin mixing near the surface; therefore, we use the most general s self-energy including $\Sigma_{\uparrow\uparrow}$, $\Sigma_{\downarrow\downarrow}$, $\Sigma_{\uparrow\downarrow}$, and $\Sigma_{\downarrow\uparrow}$. This is the first use of the more general form in a CPA calculation for a semiconductor. As in the bulk CPA, alloy effects from cation p levels are small in the surface CPA; thus, only the spin-dependent, diagonal p self-energies are used and no s-p-mixing self-energies are included.

The self-energies can be considered to be site-dependent for N layers near the surface and to be the bulk self-energies at all other sites. Calculations have been performed for $N=0$, 1, and 2. The iterative, average-t-matrix approach of Chen[6,26] is used to find self-consistent self-energies. All of the self-energies are determined simultaneously. No more than five iterations are needed to get accurate solutions. The solutions were obtained at energies with finite imaginary part ($\omega_I=0.26$ eV) to speed convergence, and the results were analytically continued to the real axis ($\omega_I=0.01$ eV) with the procedure of Hass *et al.*[27] No difficulties occurred in finding site-dependent self-energies or in performing the analytic continuations, even though structure in the surface-site self-energies and surface density of states is more singular than in the bulk self-energies and DOS.

The use of the SDCPA to study surface states in semiconductor alloys has been tested by comparing[5,6] the results of SDCPA calculations for alloys modeled as terminated one-dimensional chains with results obtained using the embedded-cluster approach for the same models. For one-dimensional models, clusters embedded at the end of the chains can be chosen large enough to give an accurate description of the surface density of states. Although the SDCPA does not reproduce the fine detail in the embedded-cluster DOS, the SDCPA does predict qualitatively correctly the large-scale structure, such as the bimodal character of the surface DOS, seen in the embedded-cluster DOS. The SDCPA should reliably model alloy effects on surface states. The VCA is unable to reproduce these results and will not always be adequate.

C. The renormalization-decimation approach

The Green's-function approach is used to implement the CPA and to determine the bulk and surface DOS. Translational symmetry parallel to the surface exists when the alloy is modeled with the VCA or CPA. Thus, the alloy Hamiltonian is diagonal in surface-wave vector, $\mathbf{k}_s$, and the calculation can be reduced by use of a Bloch representation to a set of one-dimensional-chain calculations, one for each $\mathbf{k}_s$ in the surface Brillouin zone (SBZ).[8,28] Each site in the one-dimensional chain represents a plane of equivalent sites in the crystal. The Hamiltonian for a specific site in the chain, $H_{i,i}(\mathbf{k}_s)$, describes electrons in the ith plane with surface-wave vector $\mathbf{k}_s$ (see Fig. 2). $H_{i,i}(\mathbf{k}_s)$ is a 16×16 matrix defined with the unit cell of an adjacent cation and anion in the ith plane and a $\mathbf{k}_s$ Bloch representation for the states. Coupling between adjacent planes is described by hopping matrices, $H_{i,i\pm1}(\mathbf{k}_s)$, which are also defined with the $\mathbf{k}_s$ representation. For each $\mathbf{k}_s$, the one-dimensional-chain Green's function is determined and the total-crystal Green's function is determined by summing the contribution from each $\mathbf{k}_s$ in the SBZ.

The Green's function for a one-dimensional chain with nearest-neighbor coupling is found by use of the renormalization-decimation (RD) technique.[6,8,28] In this approach every other atom on the finite chain is removed (decimation) and the Hamiltonian is renormalized to account for the decimation (see Fig. 2). The procedure is exact. After N iterations, a chain with $2^{N+1}+1$ atoms is simplified to one with three renormalized atoms, one each for the cation and anion surfaces and one for the bulk. The simpler problem is then easy to solve.

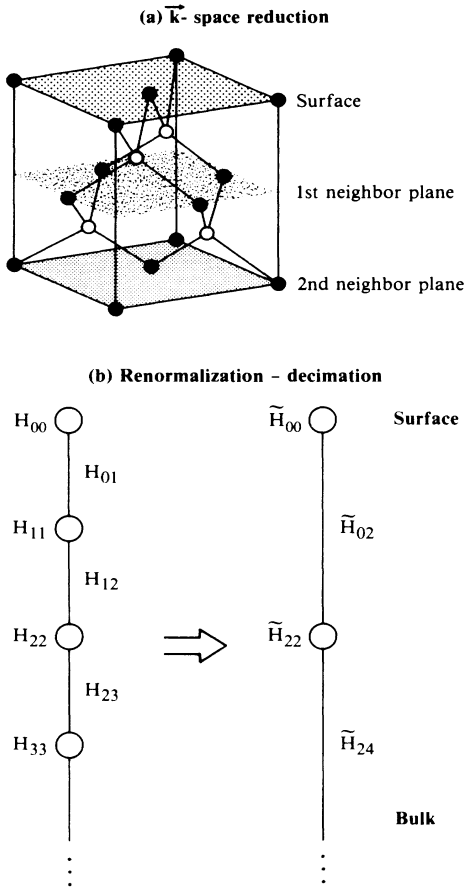

FIG. 2. (100) surface with the surface, and first- and second-neighbor planes indicated (a). In the k-space reduction these planes are reduced to a set of sites on a one-dimensional chain. An adjacent solid and open circle in (a) represent the cation and anion which define the unit cell used in the Bloch representation. The one-dimensional chain can be transformed to a simpler system using the renormalization-decimation approach as shown (b).

The renormalization prescription for removing site i from the chain is

$$\tilde{H}_{i+1,i+1}(\mathbf{k}_s)=H_{i+1,i+1}(\mathbf{k}_s)-H_{i+1,i}(\mathbf{k}_s)[\omega-H_{i,i}(\mathbf{k}_s)]^{-1}H_{i,i+1}(\mathbf{k}_s)\ , \tag{1}$$

$$\tilde{H}_{i-1,i-1}(\mathbf{k}_s)=H_{i-1,i-1}(\mathbf{k}_s)-H_{i-1,i}(\mathbf{k}_s)[\omega-H_{i,i}(\mathbf{k}_s)]^{-1}H_{i,i-1}(\mathbf{k}_s)\ , \tag{2}$$

and

$$\tilde{H}_{i+1,i-1}(\mathbf{k}_s)=-H_{i+1,i}(\mathbf{k}_s)[\omega-H_{i,i}(\mathbf{k}_s)]^{-1}H_{i,i-1}(\mathbf{k}_s)\ , \tag{3}$$

where H ($\tilde{H}$) are the Hamiltonian matrices before (after) renormalization and a similar equation defines $\tilde{H}_{i-1,i+1}(\mathbf{k}_s)$. The details of this exact procedure are given in Refs. 6 and 28. The procedure can also be understood heuristically. The correction term in Eq. (1) is the correction to motion in the $i+1$th plane that results when the electron hops to the adjacent plane ($H_{i+1,i}(\mathbf{k}_s)$), moves in the ith plane $[(\omega-H_{i,i}(\mathbf{k}_s)]^{-1}$ and then hops

back to the $i+1$th plane ($H_{i,i+1}(\mathbf{k}_s)$). In one decimation step, every other atom on the chain can be eliminated if the sites are equivalent because the same renormalization terms can be used for each eliminated atom. This simplification allows one to reduce a finite chain with $2^{N+1}+1$ atoms to a renormalized chain with three atoms in only N renormalizations.

When some of the atoms are inequivalent, for example, those at sites near the surface where the CPA self-energy is site-dependent, the renormalization-decimation approach can still be used to reduce the bulk of the system, where the atoms are equivalent, to a small, renormalized system. Other planes near the surface, which must be treated differently, can be coupled to the renormalized system. The details are given in Ref. 6.

The value of the RD approach is illustrated by comparing the (100)-ideal-cation-surface DOS at the zone center Γ in the SBZ for HgTe and CdTe slabs of different thicknesses (see Fig. 3). Performing 2, 6, 10, and 12 renormalizations provides results for films with 9, 129, 2049, and 8193 planes, respectively. The discrete structure in the surface DOS of the thin slab ($N=2$) makes

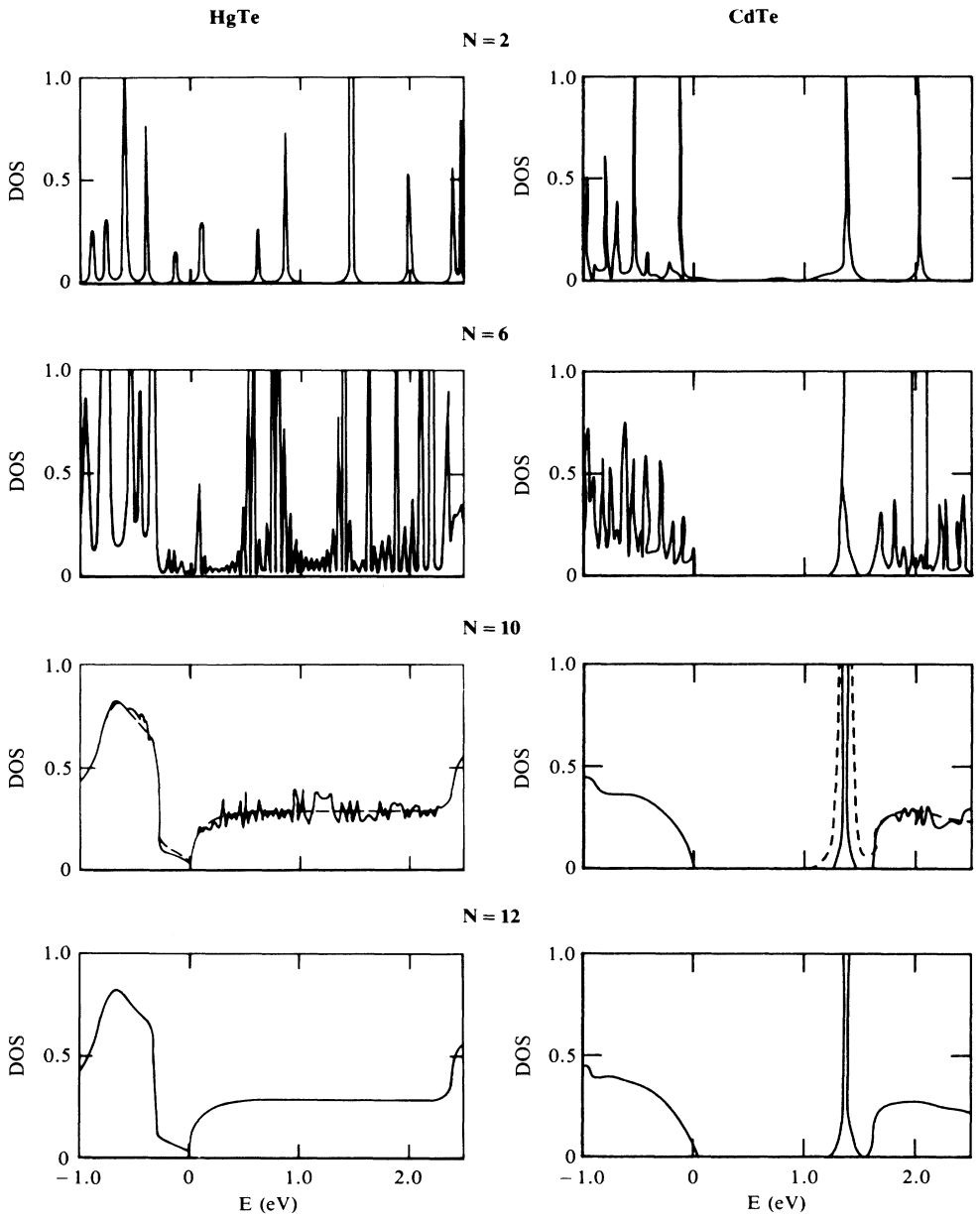

FIG. 3. Surface densities of states at Γ in the SBZ for ideal, (100), HgTe and CdTe, cation surfaces. Calculations are done with 2, 6, 10, and 12 renormalizations corresponding to slabs with 9, 129, 2049, and 8193 planes. The solid curves were all obtained by evaluating the Green's function at energies with a small imaginary part ($\omega_I=0.001$ eV). For the dashed curves $\omega_I=0.01$ eV.

identification of surface and bulk states impossible. In addition, the two slab surfaces in the thinnest slab interact with each other. The weak structure in the CdTe DOS just below 1 eV disappears as N increases. For a film with ~ 100 layers, the discrete structure is still present and makes identification of band edges (especially for HgTe) difficult. When the film has ~ 2000 layers, most of the discrete structure has been broadened away. This is more true for the valence band than for the conduction band and more for CdTe than for HgTe because the states are more local in character in each case. The discrete structures disappear completely when $N=12$. DOS that are almost identical to the DOS obtained with 12 renormalizations can also be obtained with 10 renormalizations if a larger imaginary energy is used to define the Green's function. All of the calculations reported here used ten renormalizations and were evaluated at an imaginary energy $\omega_I=0.26$ eV, but were analytically continued to $\omega_I=0.01$ eV.

Thick slabs ($\gtrsim 1000$ layers) are needed to provided realistic representations of the bulk and to eliminate surface-surface interactions and discrete structure. However, use of the full-slab matrices would be prohibitive. The renormalization procedure is effective because all matrix operations deal with small (16×16) matrices rather than matrices which describe the full slab. The decimation procedure is very efficient because N steps provide results for slabs with $2^{N+1}+1$ layers. Normal recursion methods, which build films layer by layer, build a film with only N layers after N steps. One drawback of the RD approach is that the procedure is energy-dependent and has to be performed for each energy of interest. In practice, this is not a problem for alloys because the CPA self-energies must be found for each energy anyway.

III. RESULTS

The results presented are for ideal, (100), cation, and anion surfaces of $Hg_{1-x}Cd_xTe$ with $x=0$, 0.2, 0.5, 0.8, and 1.0. The (100) surfaces were chosen because they are simpler to study than (110) or (111) surfaces when using the RD approach, and because with the RD procedure, one can simultaneously study the cation and anion surfaces which should exhibit strong and weak alloy effects, respectively. No surface relaxation or reconstruction, surface or bulk ordering, segregation or clustering, or charge transfer not in the TB model have been included because available information on $Hg_{1-x}Cd_xTe$ surfaces is inadequate. Hg is very mobile in $Hg_{1-x}Cd_xTe$. Real surfaces are likely to have cation vacancies near the surface or changes in composition near the surface. These effects will be considered elsewhere.[29]

The valence- and conduction-band edges and the surface states in the main gap of cation (100) HgTe, CdTe, and $Hg_{0.5}Cd_{0.5}Te$ surfaces are shown in Fig. 4. The surface-state energy and bulk band edges at a given $\mathbf{k}_s$ are identified as the peak of the surface-state feature in the surface DOS and the band edge in the bulk or surface DOS since alloy broadening does not smear out the structures (see Fig. 5).

The conduction-band edges and surface states of HgTe and CdTe are similar except that the CdTe states are shifted upward by 1—1.5 eV. This is a reflection of the 1.44-eV shift between Hg and Cd s-level energies. In the alloy, the VCA and CPA valence-band edges are identical because the states are anion-derived. The VCA and CPA conduction-band edges near Γ are also similar. They are different near the zone edges where the conduction-band states have less dispersion and are more local in character. However, the VCA and SDCPA surface states are very different. While the VCA-alloy surface-state band is approximately the average of the constituent surface-state

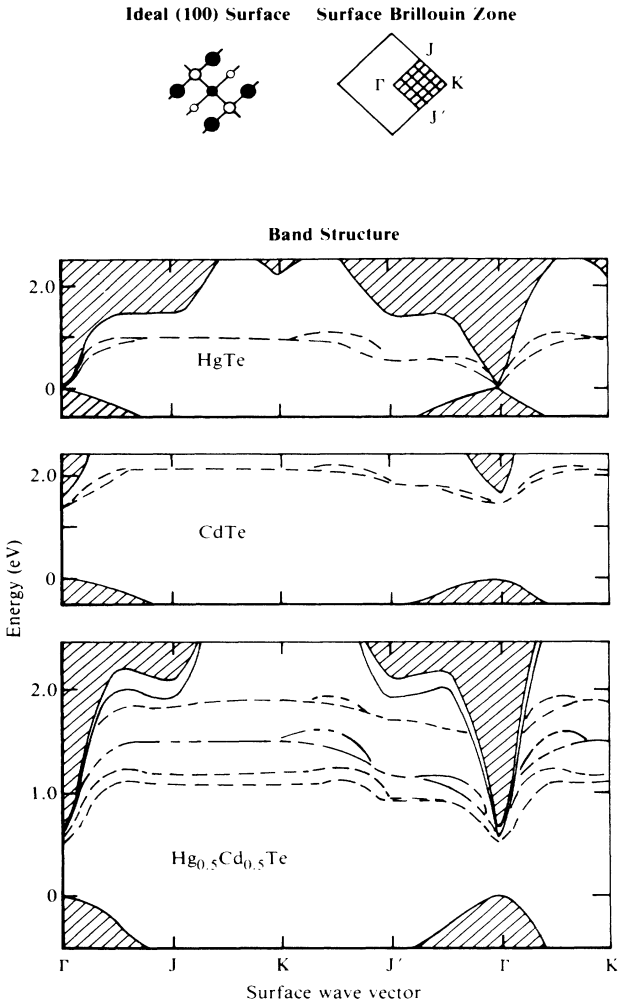

FIG. 4. Bulk and surface-state band structures projected onto the surface Brillouin zone for HgTe, CdTe, and $Hg_{0.5}Cd_{0.5}Te$ with cation-terminated, (100), ideal surfaces. The cross-hatched region indicates the bulk bands for HgTe and CdTe and the VCA bulk bands for the alloy. The shifted solid curves are the CPA band edges. The dashed curves are the surface-state bands for HgTe and CdTe and the CPA surface-state bands for the alloy. The long-short dashed curve is the VCA surface-state band. The irreducible sector of the surface Brillouin zone and the first four layers of a (100) surface are also shown. The solid (open) circles are cations (anions); the largest circles are closest to the surface, and the nearest-neighbor bonds are shown.

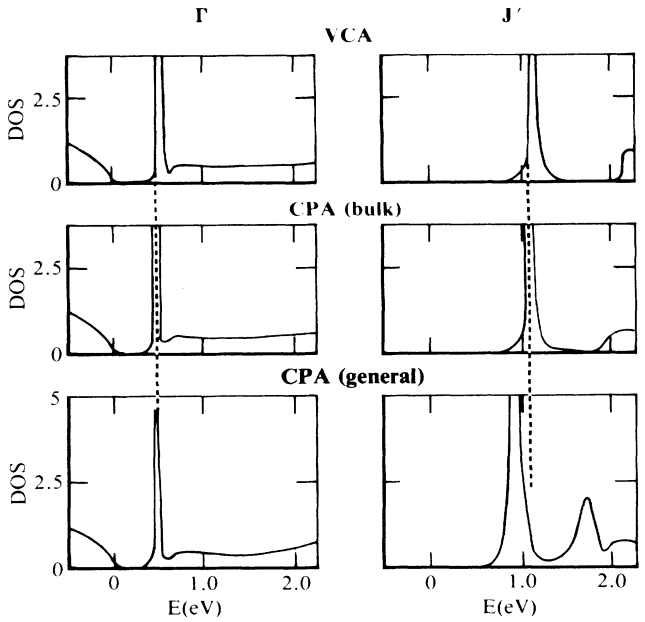

FIG. 5. Surface density of states at Γ and J' in the surface Brillouin zone found by using the VCA, the bulk CPA in which the bulk self-energy is used at all sites and the generalized SDCPA.

bands, the surface states found using the general site-dependent CPA retain the character of the constituent surface-state bands. The CdTe-like band occurs at slightly lower energies in the alloy than in CdTe because of extra repulsion from the conduction band, which is lower in the alloy. Conversely, the HgTe-like band is at higher energies in the alloy. This bimodal surface-state structure was seen in previous model surface-state calculations.[6] One can see immediately why the VCA should fail for these cation-surface states of the alloy. Because the HgTe surface states are approximately 1 eV lower than the CdTe surface states, there is little overlap between the HgTe and CdTe surface-state bands. Moreover, the states are sensitive to local alloy effects since they have little dispersion in much of the SBZ.

The bimodal structure is a direct result of the enhancement of the alloy effects at the cation surface. There is no bimodal character in the bulk near the valence-band edges, and only a small shift exists between the VCA and CPA bulk conduction-band edges, except near the zone edges where the bands have less dispersion. The site-dependent results shown in Fig. 4 were obtained with the assumption that only the surface-site self-energies were different from the bulk self-energies. Qualitatively similar results are obtained if the self-energies are different for the first two layers. However, the SDCPA must be used to get a correct description of these surface states. When the bulk self-energies are used for all sites, the bimodal structure disappears (see Fig. 5). The bulk CPA predicts a single surface state just below the VCA surface state because the bulk self-energy and the VCA energy are so close (see Fig. 6). The VCA, bulk CPA, and SDCPA do yield similar results near Γ, with the states only shifted to slightly lower energy in the more sophisticated approaches, because the states have large dispersion and are not too sensitive to alloy effects. However, even at Γ, the enhancement in the DOS above 1.5 eV, found with the SDCPA, may be a remnant of the CdTe-like state resonant with the conduction band.

The cation-surface site s self-energies shown in Fig. 6 also reflect the surface enhancement of the alloy effects and the bimodal character of the surface-state structure. The real part of the diagonal, cation-surface s self-energy ($\Sigma_{\uparrow\uparrow}$ and $\Sigma_{\downarrow\downarrow}$, where $\Sigma_{\uparrow\uparrow}=\Sigma_{\downarrow\downarrow}$), which is the effective energy of the cation s level, has large shifts to Hg-like ($E_{\mathrm{Hg}\,s}=-1.32$ eV) and to Cd-like ($E_{\mathrm{Cd}\,s}=0.12$ eV) values when the surface states are HgTe- and CdTe-like, respectively. In contrast, the real part of the bulk, diagonal self-energy shifts only slightly from the VCA energy except at higher energies (~ 2.0 eV). This slight shift is the signature of the small band-gap narrowing predicted by the CPA.[1,2] The imaginary part of the bulk, diagonal s self-energy, which gives the alloy broadening, is also

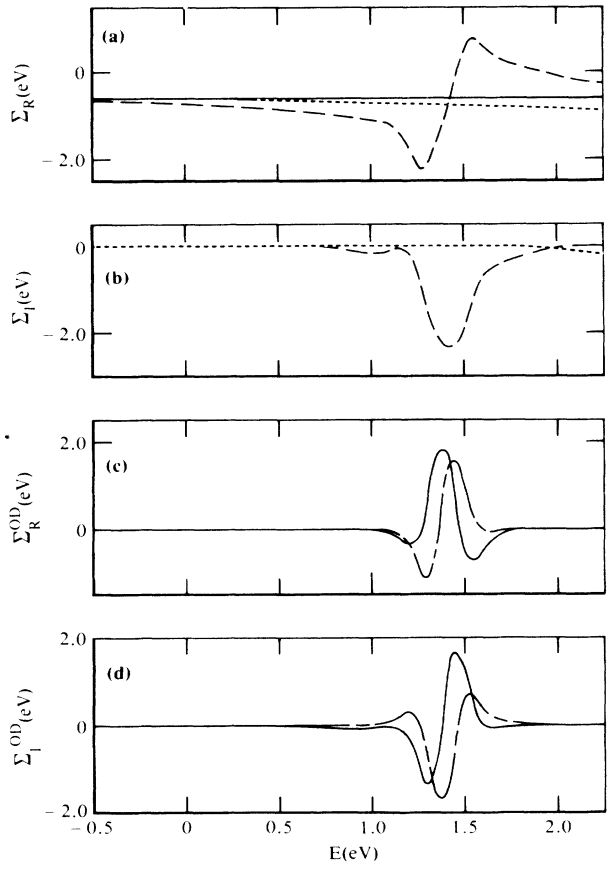

FIG. 6. The CPA cation s-level self-energy: the real (a) and imaginary (b) parts of the diagonal self-energy (each part is the same for both spins) for the VCA bulk (solid curve), CPA bulk (dotted), and CPA cation-surface site (dashed); and the real (c) and imaginary (d) parts of the off-diagonal self-energy at a cation-surface site. Both spin-mixing terms are shown.

small except at high energies. However, the alloy broadening at the cation surface can be several orders of magnitude greater than the broadening in the bulk, especially for states in the region between 1.0 and 2.0 eV, and any VCA-like structure should be broadened away. The p self-energies are not shown because the real parts differ from the VCA energies by no more than 0.01 eV and the imaginary parts are negligible. The self-energies at the cation site closest to the anion surface are not shown either. The real part of the diagonal self-energy is closer to the VCA energy for the cation site next to the anion surface than for a bulk site.

The off-diagonal, bulk s self-energies, $\Sigma_{\uparrow\downarrow}$ and $\Sigma_{\downarrow\uparrow}$, are less than 0.01 eV throughout the energy range shown, so neglect of them in bulk CPA calculations is reasonable.[1,2] However, the off-diagonal, cation-surface s self-energies are large, comparable in magnitude to the diagonal self-energies, and reflect the bimodal structure in the surface states. While the diagonal self-energies are spin-independent and the two bulk, spin-mixing self-energies are simply related (one is the negative of the other), the spin-mixing self-energies at a cation surface are not simply related. Not only is the alloy-induced spin-mixing enhanced at the surface, but the symmetry is broken as well. Nonetheless, the two spin DOS are still equal. As in the bulk, the spin-mixing self-energies at the cation site closest to the anion surface are small, although the bulk symmetry between the spin-mixing terms is broken even at the anion surface.

The x dependence of the bulk DOS and the cation surface DOS near the valence- and conduction-band edges is shown in Fig. 7. As x decreases (alloy becomes more HgTe-like) the conduction-band DOS shifts to lower energies, the bulk band gap closes, and the valence-band DOS shifts slightly to lower energies as well. The bimodal character of the surface DOS is apparent at each concentration. At small x, the HgTe-like surface-state DOS is much greater than the CdTe-like DOS. At $x=0.5$, the two bands are comparable in magnitude; at $x=0.8$, the CdTe band is dominant. Moreover, structure seen in the HgTe-like band at $x=0.2$ is broadened away as x increases. Similarly, additional structure in the CdTe band appears as x increases. Finally, there is a shift of the surface-state DOS to higher energies as x increases because the bulk conduction bands shift to higher energies.

The x dependence of the real part of the bulk and cation-surface s-level self-energies is shown in Fig. 8. The bulk self-energy for $x=0.5$ deviates the most from the corresponding VCA energy and the surface self-energy for $x=0.5$ shows the largest variation, as expected, since alloy effects are largest for $x=0.5$. For each x, the surface self-energy is bimodal and the variation in the surface self-energy is much greater than the variation in the corresponding bulk self-energy; this indicates that the surface enhancement of alloy effects occurs at each x. One might expect the structure in surface self-energy to follow the surface DOS and shift to higher energies as x increases; however, just the opposite occurs. For $x=0.2$, the struc-

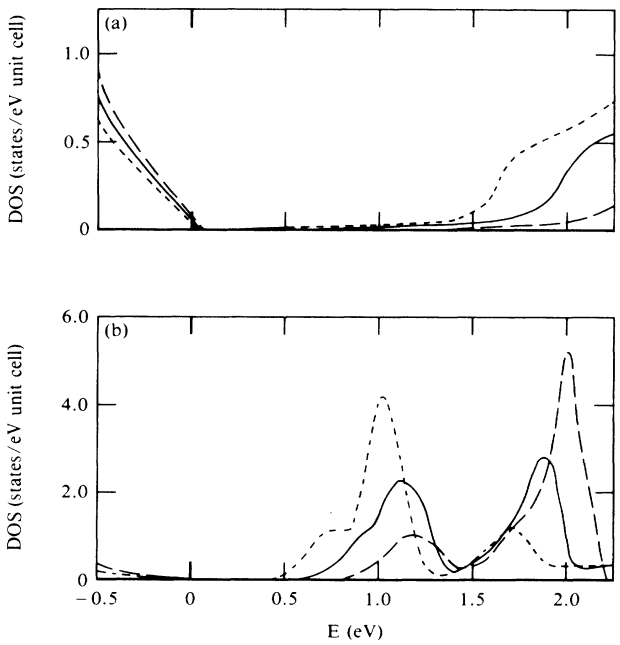

FIG. 7. x dependence of the bulk (a) and (100), cation surface (b) density of states: $x=0.2$ (dotted curve), $x=0.5$ (solid curve), and $x=0.8$ (dashed curve).

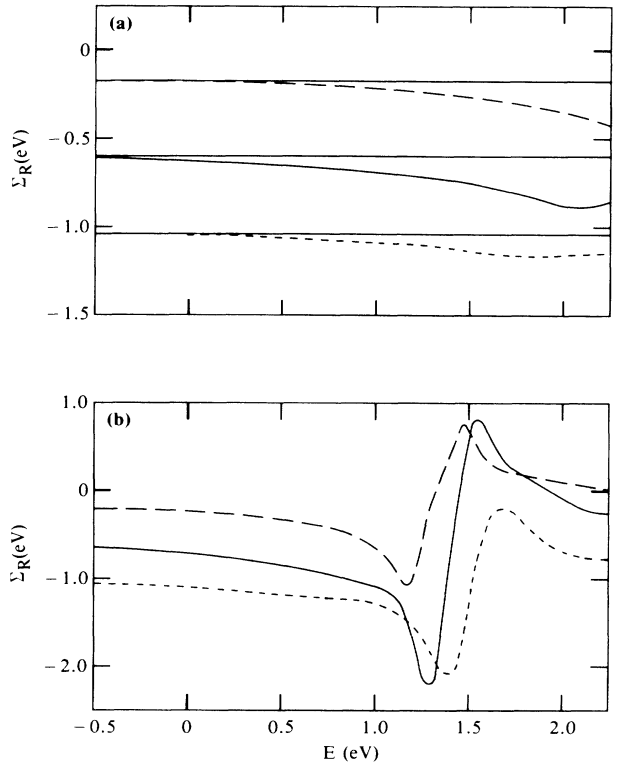

FIG. 8. x dependence of the bulk (a) and cation-surface (b) real self-energies: $x=0.2$ (dotted curve), $x=0.5$ (solid curve), and $x=0.8$ (dashed curve). The solid straight lines are the corresponding VCA energies.

ture occurs at higher energy so that the widest energy region in which $\Sigma_R \approx E_{\mathrm{Hg}\,s}$ coincides with the HgTe-like band. Similar for $x=0.8$, the structure is at lower energies so that the wide energy region in which $\Sigma_R \approx E_{\mathrm{Cd}\,s}$ coincides with the CdTe-like band. There is no dominant constituent for $x=0.5$, so the structure occurs at energies between the surface-state bands.

The density of states at bulk cation and anion sites, and at the cation and anion sites closest to the (100) cation and anion surfaces of $Hg_{0.5}Cd_{0.5}Te$ are shown in Figs. 9 and 10. Results obtained with the VCA and the SDCPA are shown for comparison. The DOS in the valence band within 3 eV, of the valence-band maximum are identical for both approximations. In the region below -4 eV, the CPA predicts a bimodal bulk DOS different from the VCA-DOS as a result of deep valence states that are local in character. This structure was first predicted by Spicer *et al.*[1] and Hass *et al.*[2] This bimodal bulk structure is also present in the DOS at the cation and anion sites closest to the anion surface and at the anion site closest to a cation surface but not at the cation site on a cation surface. The differences between the VCA and the SDCPA in the conduction band and the cation-surface-state band are obvious. The surface-state DOS at both cation and anion sites near a cation surface are bimodal in character. In contrast, the anion-derived surface-state DOS at the anion surface is the same for both approximations.

In the main band gap the surface-state DOS at the cation (anion) site on the cation (anion) surface is greater than the surface-state DOS at the adjacent anion (cation) site. Thus, the surface states in the main gap are dangling-bond states. Back-bonded surface states exist deeper in the valence band between -4.0 and -3.0 eV. At these energies the DOS at the site next to the surface is greater than the DOS at the surface site. In the VCA, which has no alloy broadening, the back-bonded surface states contribute structure to the cation-surface total DOS (see Figs. 9 and 10). In the SDCPA, the alloy disorder

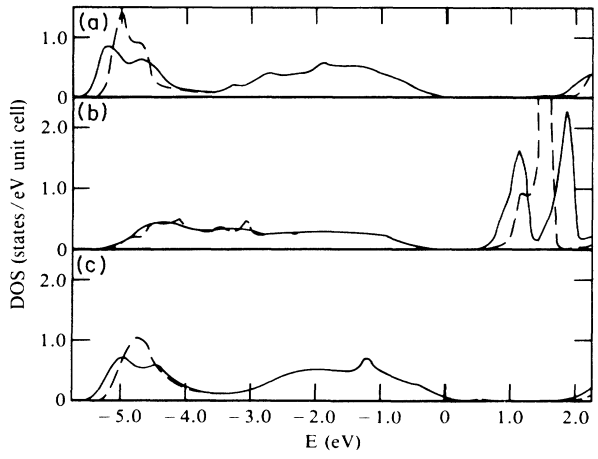

FIG. 9. Local density of states at a cation site: (a) in the bulk, (b) at the (100) cation surface, and (c) closest to the (100) anion surface. The solid curve is found by using the SDCPA, the dashed curve shows the differences predicted by the VCA.

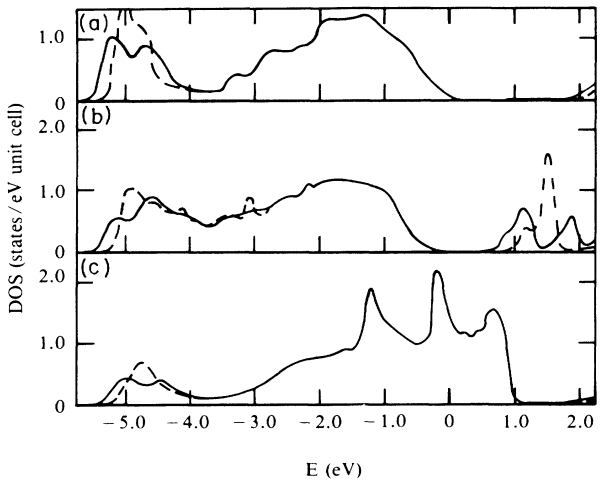

FIG. 10. Local density of states at an anion site: (a) in the bulk, (b) closest to the (100) cation surface, and (c) at the (100) anion surface. The solid curve is found by using the SDCPA, the dashed curves show the differences predicted by the VCA.

broadens away this structure in the total DOS. However, the back-bonded surface states can be identified in the DOS for fixed $\mathbf{k}_s$ when $\mathbf{k}_s$ is near a zone edge. At these $\mathbf{k}_s$ the valence-band DOS has energy gaps where the back-bonded states can exist. The back-bonded states are VCA in character with no bimodal structure. One would expect this for back-bonded states at the cation surface since these surface states are anion-derived. Back-bonded states at the alloy anion surface are difficult to identify because they are resonant with the valence band.

The self-energies in the deep valence region are shown in Fig. 11. The bulk self-energy has bimodal structure at the energies where the bulk DOS is bimodal. The bimodal variation of the bulk self-energy is weaker than the bimodal variation of the cation-surface self-energy in the main gap (Fig. 6). However, the cation-surface self-energy shows little variation at deep valence energies. Similarly, the bulk alloy broadening (Σ_I) is much larger than the cation-surface Σ_I for $E<-4.5$ eV. For -4.5 eV $\leqq E \leqq -3.0$ eV there is a small finite cation surface Σ_I that provides the alloy broadening to wash out the back-bonded state structure. The bulk and cation-surface, off-diagonal, spin-mixing self-energies are large in those energy regions where alloy effects are significant; $E \leqq -4.5$ eV for bulk states and -4 eV $\leqq E \leqq -3$ eV for the back-bond surface states. However, the variations are smaller than those shown in Fig. 6 for main gap surface states.

Several features of our implementation of the SDCPA have been tested to determine their effect on the results. The most important feature to consider is the site dependency of the self-energy. Use of the bulk self-energy at the surface site yields qualitatively incorrect results. All of the results presented here were obtained with the approximation that only the self-energy at the cation site closest to the surface was different from the bulk self-energy. We have also performed calculations by letting the two cation sites closest to the surface differ from the

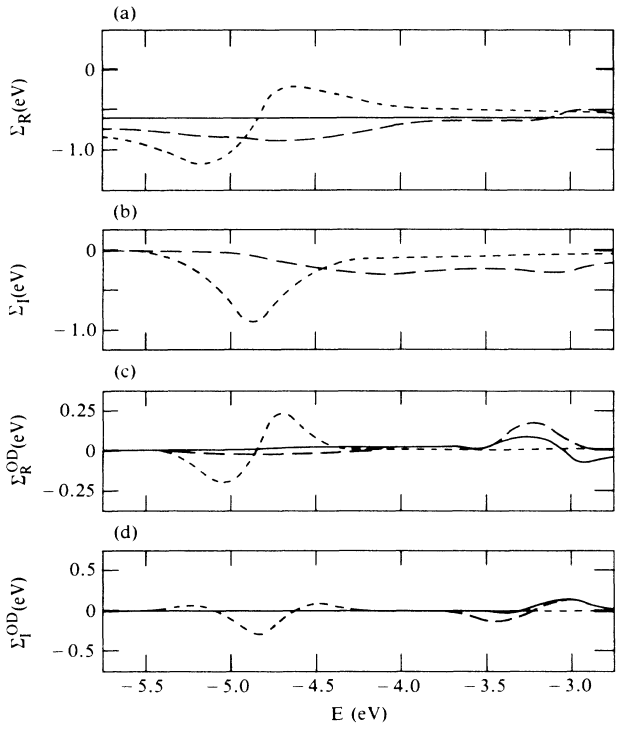

FIG. 11. The CPA cation s-level self-energy deep in the valence band: the real (a) and imaginary (b) parts of the diagonal self-energy for the VCA bulk (solid curve), CPA bulk (dotted), and CPA cation-surface site (dashed), each self-energy is the same for both spins; and the real (c) and imaginary (d) parts of the off-diagonal self-energy in the bulk (dotted curve) and at a cation-surface site (dashed and solid curves).

bulk. We get results qualitatively identical to the results found when we assumed that only the surface site was different. The self-energy at a site not on the surface is very similar to the bulk self-energy, so the healing of the self-energy occurs in the first two layers. Inclusion of the site dependency in the model is critical to obtain reliable results. However, to obtain qualitatively correct results, only the surface self-energy need be different from the bulk.

We have included off-diagonal spin mixing in the self-energy. When alloy effects are large, the off-diagonal self-energies can be comparable to the diagonal self-energies. We have also performed the calculations for $x=0.5$ by ignoring the off-diagonal self-energies. We get similar results with and without the off-diagonal self-energies although structure in the DOS is sharper when the spin-mixing terms are ignored. Most of the disorder effects that are accounted for with a finite off-diagonal self-energy Σ_{od} are included when $\Sigma_{od}=0$ because the diagonal self-energy is larger when $\Sigma_{od}=0$. In addition, the splitting of the HgTe-like surface state into two states in the alloy (see Fig. 4) must be due to spin-mixing effects, since only a single surface state is seen when $\Sigma_{od}=0$.

We performed the calculations reported here by using a finite p-level self-energy. However, disorder in the p level should have little effect on the results. There was little quantitative change when the VCA p-level energy was used for the p self-energy. However, in other contexts, for example when cation vacancies at the surface are included,[29] the p-level self-energy must be treated more carefully.

We have tested the importance of including in the calculations the site dependence of the self-energy, the spin-mixing effects, and the p-level self-energy. Only the site dependency must be included to obtain a correct description of the alloy effects. The spin-mixing effects and the p-level self-energies can be ignored in our calculations, thus simplifying the calculations, without affecting the results.

IV. CONCLUSIONS

Calculations of the electronic structure of bulk $Hg_{1-x}Cd_xTe$ and the surface states of the ideal (100) cation and anion alloy surfaces have been performed by employing the site-dependent coherent-potential approximation. Well-extended states are accurately described with the virtual-crystal approximation. States that are more local in character are more sensitive to alloy disorder effects and must be described with more sophisticated alloy models such as the SDCPA. Alloy effects on deep valence bulk states are enhanced because of the local character of the states. The enhancement of alloy effects is even greater for surface states that are sensitive to cation occupation because surface states are truly localized in one direction. The signature of this enhancement is the appearance of bimodal structure in the density of states and the self-energies. The surface states retain the character of the constituent surface states rather than take on the character of virtual-crystal effective cations. This bimodal structure appears not just for concentrations where alloy effects should be greatest, but also for concentrations where alloy effects should be weak.

Great care should be taken in analyzing alloy effects on localized states. Those states insensitive to the disordered sites, such as dangling-bond states at anion surfaces and back-bonded states, can be described with the VCA. Those states that are sensitive to the disordered sites, such as the dangling-bond states at cation surfaces, can only be described with a site-dependent CPA. Both the VCA and the bulk CPA yield qualitatively incorrect results for these states. The choice of an effective alloy model depends not only on the constituents of the alloy but also on the states to be studied, the extent of their localization, and their sensitivity to disordered sites.

ACKNOWLEDGMENTS

This work was performed under the McDonnell Douglas Corporation Independent Research and Development program. The author would like to thank H. Atkins, R. Whitaker, J. Putnam, and D.-S. Wang for help in the numerical analysis and M. Uram and P. Newell for help in the computing. Discussions with D. Papaconstantopoulos and K. C. Hass are also gratefully acknowledged. The author would also like to thank K. C. Hass for providing a copy of his thesis.

[1]W. E. Spicer, J. A. Silberman, J. Morgen, I. Lindau, J. A. Wilson, A.-B. Chen, and A. Sher, Phys. Rev. Lett. **49**, 948 (1982).
[2]K. C. Hass, H. Ehrenreich, and B. Velický, Phys. Rev. B **27**, 1088 (1983).
[3]M. Janos and P. S. Guimarães, J. Phys. C **18**, L117 (1985).
[4]N. F. Berk, Surf. Sci. **48**, 289 (1975).
[5]G. W. Bryant, Surf. Sci. **154**, 435 (1985).
[6]G. W. Bryant, Phys. Rev. B **31**, 5166 (1985).
[7]M. C. Desjonquères and F. Cyrot-Lackman, J. Phys. F **7**, 61 (1977).
[8]G. W. Bryant, Phys. Rev. Lett. **55**, 1786 (1985).
[9]See R. E. Allen and J. D. Dow, J. Vac. Sci. Technol. **19**, 383 (1981), for a list of references.
[10]R. E. Allen, H. P. Hjalmarson, and J. D. Dow, Surf. Sci. **10**, L625 (1981).
[11]R. E. Allen and J. D. Dow, Phys. Rev. B **25**, 1423 (1982).
[12]A. C. Redfield, M. A. Bowen, K. E. Newman, and J. D. Dow, Solid State Commun. **46**, 371 (1983).
[13]J. Singh and A. Madhukar, Phys. Rev. B **25**, 7700 (1982).
[14]C. A. Swarts, M. S. Daw, and T. C. McGill, J. Vac. Sci. Technol. **21**, 198 (1982).
[15]A. Kobayashi, O. F. Sankey, and J. D. Dow, Phys. Rev. B **25**, 6367 (1982).
[16]C. W. Myles, P. F. Williams, R. A. Chapman, and E. G. Bylander, J. Appl. Phys. **57**, 5279 (1985).
[17]C. Tuncay and M. Tomak, Solid State Commun. **50**, 1065 (1984).
[18]D. J. Chadi, J. P. Walter, M. L. Cohen, V. Petroff, and M. Balkanski, Phys. Rev. B **5**, 3058 (1972); J. R. Chelikowsky and M. L. Cohen, *ibid.* **14**, 556 (1976).
[19]W. Walukiewicz, J. Phys. C **9**, 1945 (1976).
[20]J. I. Pankove, *Optical Processes in Semiconductors* (Dover, New York, 1974), p. 412.
[21]D. J. Chadi, Phys. Rev. B **16**, 790 (1977).
[22]P. Soven, Phys. Rev. **156**, 809 (1967).
[23]R. J. Elliott, J. A. Krumhansl, and P. L. Leath, Rev. Mod. Phys. **46**, 465 (1974).
[24]H. Ueba and S. Ichimura, Phys. Status Solidi B **92**, 307 (1979).
[25]A. Zagorski and W. Nazarewicz, Acta Phys. Pol. **A57**, 403 (1980).
[26]A.-B. Chen, Phys. Rev. B **7**, 2230 (1973).
[27]K. C. Hass, B. Velický, and H. Ehrenreich, Phys. Rev. B **29**, 3697 (1984).
[28]M. P. López Sancho, J. M. López Sancho, and J. Rubio, J. Phys. F **25**, 851 (1985), other references to the renormalization-decimation approach are given in this paper and Ref. 6.
[29]G. W. Bryant (unpublished).